12th International Conference on Heat Transfer, Fluid Mechanics and Thermodynamics
Costa Del Sol, Spain 11-13 July 2016

GENERALIZED DRAINING FILM MODEL EQUATION SET TO EXECUTE AN EXACT NUMERICAL SOLUTION FOR CFD CODE VALIDATION

Xiao J.*, Travis J. and Bottoni M.
*Author for correspondence
Institute of Nuclear and Energy Technologies,
Karlsruhe Institute of Technology,
P.O. Box 3640, 76021 Karlsruhe, Germany
E-mail: jianjun.xiao@kit.edu

ABSTRACT

The Westinghouse Advanced Passive PWR AP-600 and AP-1000 are pressurized water reactors (PWR) with advanced passive safety systems. Most recognize the passive containment cooling system (PCCS) as being one of the most important concepts for advanced passive safety systems. The steel containment structure consists of a vertical right-circular cylinder capped with oblate spheroids at both ends. Following a postulated design-base-accident (DBA), an outside cold liquid-water spray is injected on the apex of the spheroidal dome. The resulting liquid-film drains under gravitational body forces over the outside dome surface and down the cylinder surface. This PCCS removes heat from the containment interior to reduce potentially damaging pressure and temperature loads. To facilitate model validation we have developed an exact numerical solution (ENS) for the one-dimensional steady-state liquid film flow over an ellipsoidal-domed cylinder. Although the ENS assumes constant containment wall temperature and outside ambient air temperature, it can incorporates any generalized heat transfer correlation between the containment surface and liquid film as well as any generalized heat and mass (evaporation) transfer correlations between the film and outside ambient air. ENS results for draining liquid water films clearly present the coupling effects of heat and mass transfer.

NOMENCLATURE

C	[kJ/kg·K]	Specific heat.
d	[m]	PCCS drainage pipe diameter.
D	[m^2/s]	Diffusion coefficient.
g	[m/s^2]	Gravitational constant.
h	[m]	Minor semi-axis of the AP600 and AP1000 ellipsoidal dome.
h	[kJ/kg]	Heat of vaporization.
h	[W/m^2·K]	Heat transfer coefficient.
I	[kJ/kg]	Film specific internal energy.
k	[W/m·K]	Film thermal conductivity.
L	[m]	Length of the AP600 and AP1000 vertical right circular cylinder.
$\dot{m}$	[kg/s]	Mass flow of the injected cold water.
P	[Pa]	Pressure.
P	[m,m]	Point on the ellipsoidal surface.
Pr	[-]	Prandtl Number.
r	[m]	Radial coordinate of the ellipsoidal dome.
R	[m]	Major semiaxis of the AP600 and AP1000 ellipsoidal dome.
R	[kJ/kg·K]	Gas constant.
Re	[-]	Reynolds Number.
s	[m]	Surface coordinate directed along a meridian.
S	[kg/m^2·s]	Mass equation source term.
S	[kJ/ m^2·s]	Energy equation source term.
S	[$kg/m·s^2$]	Momentum equation vector source term.
Sc	[-]	Schmidt Number.
t	[s]	Time.
T	[K]	Average film temperature.
$\boldsymbol{u}$	[m/s]	Average film velocity vector.
u	[m/s]	Average film velocity along a surface meridian.
x	[m]	Coordinate.
X	[m]	Coordinate direction.
y	[m]	Coordinate.
z	[m]	Coordinate.
Z	[m]	Coordinate direction.

Special characters

α	[kg/s]	Film mass flow rate along the dome surface meridian.
β	[kg/m·s]	Film mass flux along the cylinder surface meridian.
δ	[m]	Average film thickness.
∇	[1/m]	Divergence operator.
ϕ	[-]	Tangent of the dome ellipse with respect to the horizontal.
θ	[-]	Eccentric anomaly of any given point $P_1(x,z_1)$ on the elliptic meridian line of the dome (radians).
ψ	[-]	Anomaly of any given point P(x,z) on the elliptical dome (radians).
μ	[kg/m·s]	Film dynamic viscosity.
ν	[m^2/s]	Film kinematic viscosity.
ρ	[kg/m^3]	Film density.

Subscripts

0	Initial value
air	Ambient air
c	Reference to the vertical right circular cylinder
d	Reference to the dome ellipse of revolution
g	Reference to water vapor phase, i.e., gas phase
gas	Reference to the ambient gas phase
h_2o	Water-vapor component
ie	Reference to the energy conservation equation
mass	Reference to mass conservation equation
max	Maximum value
mom	Reference to the momentum conservation equation
n	Outward directed normal to the containment vessel wall
s	Reference to surface coordinate
sat	Saturation value
v	Constant volume
w	Reference to the outside containment vessel wall

INTRODUCTION

The Westinghouse AP600 and AP1000, two Advanced Power Reactors, utilize a passive containment cooling system to remove heat released inside the secondary containment vessel following postulated design-base accidents such as a main steam line break (MSLB) or loss-of-coolant accident. (LOCA). During a DBA, steam is released and thus pressure and temperatures increase inside the containment vessel. The major purpose of the PCCS is to reduce and control the containment's internal pressure and temperature below design values. The secondary containment vessel and PCCS is shown in **Figure 1**. The vessel itself is an ASME metal containment.

The containment vessel is a free standing right circular cylinder capped with oblate spheroids at both ends. Both AP600 and AP1000 have a diameter of 130 feet (39.6 m) with the minor vertical axis for each oblate spheroid being 37 feet 7.5 inches (11.46 m). The AP1000 cylinder is 140 feet (42.7 m) in height while the AP600 is 25.5 feet (7.77 m) less, which provides additional free volume for the AP1000. As seen in **Figure 1**, the PCCS provides cold liquid water at the outside apex of the ellipsoidal dome with a designed mass flow rate between 20 and 30 kg/s up to 72 hours. The idea is that the cold water draining over the ellipsoidal dome and down the vertical cylinder sides cools the containment vessel while inside the vessel condensing steam reduces the internal pressure and temperature.

A number of specialized safety analysis containment codes [2-4] have been developed to simulate the effects of this draining liquid water film over the past 30 years or so, but the developers had little data to validate their models. Even though there have been a number of experiments conducted by Westinghouse on small and large test facilities, the data remains largely closed to most developers. Analyses with WGOTHIC [4] are available in the open literature; however all PCCS data and simulated results have been redacted. Argonne National Laboratory was able to arrange a special agreement with Westinghouse to gain access to the raw data, but Argonne's published reports and papers provide little information [5] where all data and simulated results have been normalized to some unknown values. For this reason we attempt to develop an exact numerical solution methodology so that developers can validate the more complicated draining film models embedded in containment safety analysis computer codes.

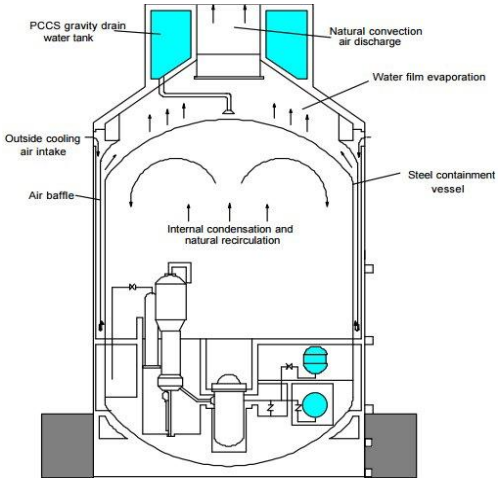

Figure 1 AP1000 containment vessel and PCCS (Courtesy of Westinghouse [1])

GEOMETRIC CONSIDERATIONS

In **Figure 2** we present a schematic diagram of the oblate ellipsoid domed cylinder. By design, the bottom ellipsoid is not represented and only an upper 82 feet (25 m) section of the cylinder is cooled by the draining film for the AP1000 while only the upper 56 feet (17 m) section is cooled in the AP600. **Table 1** gives the geometric dimensions used in this analysis.

With the cold liquid water (around 300 K) injected at the apex of the ellipsoid dome, we can envision the water draining due to gravitational body forces along an ellipsoid meridian and then transitioning to the cylinder at $\theta = \pi/2$. Therefore, we consider a solution procedure involving boundary conditions at the apex for the ellipsoid and at the cylinder transition boundary conditions equaling the ellipsoid solution at $\theta = \pi/2$. We define an oblate ellipsoid as the body of revolution of interest, centered at the origin, as

$$\frac{x^2 + y^2}{R^2} + \frac{z^2}{h^2} = 1 \quad ; R > h \tag{1}$$

which simply reduces to an ellipse (body of revolution) along any given meridian (see **Figure 2**)

$$\frac{x^2}{R^2} + \frac{z^2}{h^2} = 1 \quad ; R > h \tag{2}$$

The parametric equations of the ellipse are given in terms of the parameter θ (eccentric anomaly – see **Figure 3**) by

$$(x,z)=(R\sin\theta,h\cos\theta). \tag{3}$$

The parameter θ increases from the ellipse apex (θ=0) to the horizontal ($\theta=\pi/2$), which is the point of transition from the ellipsoid dome to the vertical cylinder. The eccentric anomaly θ is related to the anomaly ψ by

$$\psi=\tan^{-1}\left(\frac{r}{z}\right)=\tan^{-1}\left(\frac{R\sin\theta}{h\cos\theta}\right)=\tan^{-1}\left(\frac{R}{h}\tan\theta\right). \tag{4}$$

From equation (3), we obtain

$$\begin{cases} d(x)=d(R\sin\theta)=R\cos\theta d\theta \\ d(z)=d(h\cos\theta)=-h\sin\theta d\theta \end{cases} \tag{5}$$

The incremental length along a meridian in terms of the parameterized variable θ is formed as follows:

$$ds=\left(dx^2+dz^2\right)^{\frac{1}{2}}=\left(R^2\cos^2\theta+h^2\sin^2\theta\right)^{\frac{1}{2}}d\theta \tag{6}$$

which upon integration gives the famous incomplete elliptic integral of the second kind

$$s=\int_0^{\theta}\left(R^2\cos^2\theta+h^2\sin^2\theta\right)^{\frac{1}{2}}d\theta. \tag{7}$$

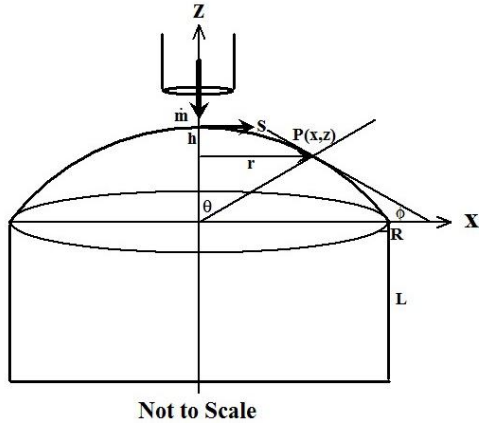

Figure 2 - A schematic representation of an oblate ellipsoid domed cylinder

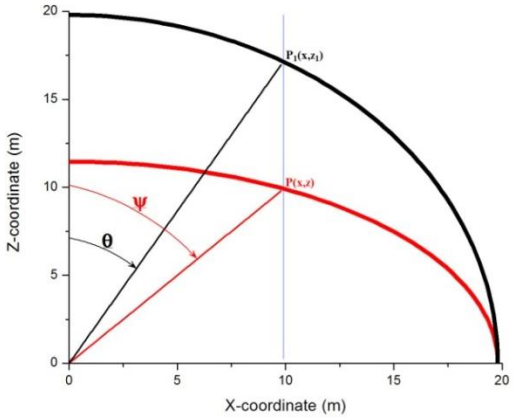

Figure 3 - Definition of eccentric anomaly θ and of anomaly ψ of a generic point P(x,z) on the elliptical meridian line of the dome.

When $\theta=\pi/2$, the integral is termed complete, and for the dimensions given in **Table** 1, the length from the ellipsoid apex along a meridian to the cylinder transition is 24.99 m (integral evaluated with MathCad 15).

The tangent along any point on the meridian measured to the horizontal ϕ is written

$$\sin\phi=\frac{|dz|}{ds}=\frac{h\sin\theta}{\left(R^2\cos^2\theta+h^2\sin^2\theta\right)^{\frac{1}{2}}}. \tag{8}$$

These relationships will be used in the developments below.

Table 1 Geometric dimensions related to **Figure 2**

	AP600	**AP1000**
h	11.46 meters	11.46 meters
R	19.8 meters	19.8 meters
L	17 meters	25 meters

In the following development and discussion, we will refer to the geometrical dimensions of the AP-1000 reactor. The only major difference between the geometry of the two reactor models, namely the height of the cylindrical vessel, is irrelevant for the analysis presented in this article.

THEORETICAL DEVELOPMENTS

The conservation of mass, momentum, and energy describing a draining film [6-8] are

$$\frac{\partial\rho\delta}{\partial t}+\nabla_s\cdot\left(\rho\delta\mathbf{u}\right)=S_{mass}, \tag{9}$$

$$\frac{\partial\rho\delta\mathbf{u}}{\partial t}+\nabla_s\cdot\left(\rho\delta\mathbf{uu}\right)=S_{mom}, \tag{10}$$

$$\frac{\partial\rho\delta I}{\partial t}+\nabla_s\cdot\left(\rho\delta\mathbf{u}I\right)=S_{ie}. \tag{11}$$

We establish that the thin liquid film flow is incompressible, steady, and draining under gravity along a meridian from the ellipsoid apex. Further that the film source is liquid water at constant mass flow rate and temperature. Upon examining the National Institute of Standards and Technology (NIST) Equation of State (EoS) for liquid water [9], we can accurately represent the internal energy in equation (11) from 280 K to the boiling point at 1 atmosphere with less than 0.2% relative error as

$$I_l=\text{-}1143.5186963699+C_v\cdot T_l \tag{12}$$

We define C_v=4.1866973442 (kJ/kg·K). Other liquid water properties such as the density, dynamic viscosity, thermal conductivity and heat of vaporization are also approximated from NIST EoS data with relative error less than 0.4% and are given in **Table 2**.

The approximating function is $\Omega(T)=\sum_{i=0}^{n}a_i\,T^i$, where $\Omega(T)$ represents each of the listed properties.

The conservation equations (9)-(11), with their respective source terms, are written

$$\frac{d}{ds}\left(r\rho\delta u\right)=\frac{d}{ds}\alpha=rS_{mass}, \tag{13}$$

$$\frac{d}{ds}\left(r\rho\delta uu\right)=\frac{d}{ds}\left(\alpha u\right)=rS_{mom}$$
$$=r\left(S_{mass}u-3\mu\frac{u}{\delta}+g\rho\delta\sin\phi\right), \quad (14)$$

$$\frac{d}{ds}\left(r\rho\delta\mathbf{u}I\right)=C_v\frac{d}{ds}\left(\alpha T\right)$$
$$=r\left[S_{mass}h_g\left(T\right)+h_{gas}\left(T_{gas}-T\right)+h_w\left(T_w-T\right)+S_{mass}C_vT\right], \quad (15)$$

where $\alpha\equiv r\rho\delta u=R\sin\theta\rho\delta u$. The s-coordinate designates flow along the meridian of the body of revolution surface (ellipsoid and then cylinder) starting at the apex, and r is the radial distance from the z-axis to the location on the surface.

Table 2. Polynomial coefficients approximating the NIST liquid-water EoS within 0.4% relative error.

	I	ρ	ν	k	h_g
	kJ/kg	kg/m^3	m^2/s	W/(m*K)	kJ/kg
n	1	3	5	3	2
a_0	1143.518696	329.6546175	1360.83728604371	-0.957375509	3032.38070257
a_1	4.186697344	5.891980833	-19.607359046740	0.0093062761	-1.5930403355
a_2	-	-0.016152345	0.11347440661614	-1.528017E-5	-0.0012990131
a_3	-	1.3073093E-5	-3.29264494664E-4	5.6025661E-9	-
a_4	-	-	4.78613861464E-7	-	-
a_5	-	-	-2.7864245376E-10	-	-

We assume the film is usually very thin (h ~ 0.1 cm) and therefore the average film bulk temperature is not much different from the interface temperatures at the wall and gas. As for the film velocity we impose a parabolic profile across the film thickness, normal to the surface tangent, from no-slip at the containment surface to free-slip at the film-gas interface which gives

$$u(y)=2u_{\max}\left(-\frac{y_n^{\,2}}{2\delta^2}+\frac{y_n}{\delta}\right), \quad (16)$$

where the coordinate y_n (along which the integration is made) is normal to the tangent to the surface of the body of revolution and directed outwardly. Integrating equation (16) over the film thickness δ, we obtain $u_{\max}=3u/2$, where $u_{\max}$ is the maximum velocity of the liquid film at its outer boundary, the film-gas interface. The assumption of the parabolic profile (16) across the liquid film implies also the assumption of a laminar flow regime.

Expanding the spatial derivatives in equations (13)-(15), the system of first order highly non-linear ordinary differential equations is

$$\frac{d}{ds}\alpha=rS_{mass}, \quad (17)$$

$$\frac{d}{ds}u=-\frac{3\nu}{\delta^2}+g\frac{1}{u}\sin\phi=-3\nu\left(\frac{R\sin\theta\rho u}{\alpha}\right)^2+g\frac{1}{u}\sin\phi, \quad (18)$$

$$\frac{d}{ds}T=\frac{r}{\alpha C_v}\left[S_{mass}h_g\left(T\right)+h_{gas}\left(T_{gas}-T\right)+h_w\left(T_w-T\right)\right], \quad (19)$$

where again $\alpha = R\sin\theta\rho\delta u$.

Equation set for flow over the ellipsoidal dome

Introducing equations (6) and (8) into (17)-(19) we obtain

$$\frac{d}{d\theta}\alpha\left(\theta\right)=R\sin\theta\left(R^2\cos^2\theta+h^2\sin^2\theta\right)^{\frac{1}{2}}S_{mass}, \quad (20)$$

$$\frac{d}{d\theta}u_d\left(\theta\right)=-3\nu\left(T_d\right)\bullet\left(\frac{R\sin\theta\rho\left(T_d\right)u_d\left(\theta\right)}{\alpha}\right)^2 \bullet\left(R^2\cos^2\theta+h^2\sin^2\theta\right)^{\frac{1}{2}}+g\frac{h\sin\theta}{u_d\left(\theta\right)}, \quad (21)$$

$$\frac{d}{d\theta}T_d\left(\theta\right)=\frac{R\sin\theta}{\alpha\left(\theta\right)C_v}\left[S_{mass}h_g\left(T_d\left(\theta\right)\right)+h_{gas}\left(T_{gas}-T_d\left(\theta\right)\right)+h_w\left(T_w-T_d\left(\theta\right)\right)\right]\cdot \left(R^2\cos^2\theta+h^2\sin^2\theta\right)^{\frac{1}{2}}. \quad (22)$$

Equation set for flow over the cylinder

An analogous system for a vertical cylinder with large diameter can be written

$$\frac{d}{dz}\left(\delta\rho u_c\right)=\frac{d}{dz}\beta\left(z\right)=S_{mass}, \quad (23)$$

$$\frac{d}{dz}u_c\left(z\right)=-3\nu\left(T_c\right)\left(\frac{\rho\left(T_c\right)u_c\left(z\right)}{\beta\left(z\right)}\right)^2+\frac{g}{u_l\left(z\right)}, \quad (24)$$

$$\frac{d}{dz}T_c\left(z\right)=\frac{1}{\beta\left(z\right)C_v}\left[S_{mass}h_g\left(T_c\right)+h_{gas}\left(T_{gas}-T_c\left(z\right)\right)+h_w\left(T_w-T_c\left(z\right)\right)\right], \quad (25)$$

where $\beta\equiv\rho\left(T_c\right)\delta_c u_c$.

Initial Conditions

A constant mass flow rate $\dot{m}$ issuing from a pipe with diameter d at a constant temperature T_0 is injected at the apex of the ellipsoid as shown in **Figure 2**. Assuming that the injection pipe is not far from the ellipsoid apex we neglect any gravitational acceleration so the initial film velocity $u_{d,0}$ is equal to the injection velocity. We compute the initial velocity

$$u_{d,0}=4\frac{\dot{m}}{\rho\left(T_0\right)\pi d^2}, \quad (26)$$

and from this we can compute the initial film thickness

$$\delta_{d,0}=\frac{\dot{m}}{\rho\left(T_{d,0}\right)\pi d u_{d,0}}=\frac{d}{4} \quad (27)$$

leading to

$$\alpha_0=R\sin\theta_0\rho\left(T_{d,0}\right)\delta_{d,0}u_{d,0}, \quad (28)$$

where $\theta_0=\sin^{-1}\left(\delta r/R\right)$. The initial conditions for the cylinder at the ellipsoid-cylinder transition are simply

$$\delta_{c,0}=\delta_d\left(\frac{\pi}{2}\right), \quad (29)$$

$$u_{c,0}=u_d\left(\frac{\pi}{2}\right), \quad (30)$$

$$T_{c,0}=T_d\left(\frac{\pi}{2}\right), \quad (31)$$

giving $\beta_0\equiv\rho\left(T_{c,0}\right)\delta_{c,0}u_{c,0}$.

SOME EXACT NUMERICAL SOLUTIONS

Integration of systems (20)-(22) and (23)-(25) are performed with MathCad 15. We present 6 cases to demonstrate the utility of this methodology. For all cases we assume the following constant parameters:

1. Injected cold water mass flow rate $\dot{m} = 25$ *kg/s*,
2. Injected cold water temperature $T = 300$ *K*,
3. Containment surface temperature $T_w = 370$ *K*,
4. Ambient gas temperature $T_{gas} = 298$ *K*, and
5. Ambient gas velocity $u_{gas} = 0$ *m/s*.

The remaining parameters are given the **Table 3**. Note that the PCCS drain pipe diameter is listed as a parameter as we have not been able to find any specifications for it.

Table 3. Definition of parameters used for the 6 Exact Numerical Solution cases

Case	Injection pipe diameter, d, (m)	Wall-film heat transfer coefficient, h_w, (W/m^2-K)	Film-gas heat transfer coefficient, h_{gas}, (W/m^2-K)	Mass transfer function, S_{mass}, (kg/m^2-s)
1	0.2	1.5E+02	0	0
2	0.2	1.5E+02	0.5E+02	0
3	0.2	1.5E+02	0.5E+02	-1.0E-03
4	0.1	1.5E+02	0.5E+02	-1.0E-03
5	0.3	1.5E+02	0.5E+02	-1.0E-03
6	0.2	Equation (32)	Equation (33)	Equation (34)

The numerical values of the heat transfer coefficients and of the mass transfer function given in Table 3 for the first 5 cases have not been suggested by the status of an operational reactor, but, conforming to the purpose of the article of developing a general methodology, they have been chosen as characteristic values in their range of variability.

In case 6 we use the same heat and mass transfer correlations that are used in our sister-paper [6] between the wall and film

$$h_w = \frac{k(T)}{\delta(s)}\left[3.2 + 2.37\cdot 10^{-4}\,\mathrm{Re}(s)\right], \tag{32}$$

film and ambient gas

$$h_{gas} = \frac{k_{gas}}{\delta(s)} 0.664\left(\mathrm{Re}_{gas}\right)^{\frac{1}{2}}\left(\mathrm{Pr}_{gas}\right)^{\frac{1}{3}}, \tag{33}$$

and mass transfer (evaporating film) function

$$S_{mass} = \rho_{gas}\left[\frac{D_{h2o\to air}}{\delta(s)} 0.664\left(\mathrm{Re}_{gas}\right)^{\frac{1}{2}}\left(Sc_{gas}\right)^{\frac{1}{3}}\right]\frac{\left(\rho_{h2o} - \rho_{sat}(T)\right)}{\left(\rho_{gas} - \rho_{sat}(T)\right)}, \tag{34}$$

where Re(s) is the film Reynolds Number, Re_{gas} is the gas Reynolds Number, Pr_{gas} is the gas Prandtl Number, Sc_{gas} is the gas Schmidt Number, and $D_{h2o\to air}$ is the molecular diffusion coefficient for water vapor into air. The saturation density $\rho_{sat}(T)$ is computed with the ideal gas equation of state with the saturation pressure

$$\rho_{sat}(T) = \frac{p_{sat}(T)}{R_{h20}\cdot T}, \tag{35}$$

where the saturation curve is approximated within a relative error of 0.2% of the NIST data by a modified Antoine Equation [10]. Note that ρ_{h2o} is the water vapor density component in the ambient gas adjacent to the draining film. Equation (34) can be maximized for evaporation by setting the local contribution for the water vapor density equal to zero. We have done this for the Case 6 simulation.

The results of the first three cases are shown in **Figures 4~6**. In these three figures we demonstrate the effects of adding:

1. Heat transfer between the containment wall and the draining film,
2. Heat transfer between the draining film and the ambient air, and
3. Mass transfer (evaporation) of the film into the ambient air.

The heat transfer coefficients and mass transfer function (a constant) were purposely selected to amplify each of the three transport mechanisms.

Radiation heat transfer was not included in our analysis because the film temperature, which does not exceed 370 K, results in a negligible radiation contribution to heat transfer with respect to the other transport mechanisms. Because of the small film thickness, the temperature drop across the liquid film is negligible with respect to the temperature gradient along the film.

We offer a few observations from these three figures:

1. As the film is cooler by adding heat transfer between film and ambient air and then film vaporization effects, we see a decrease in the film velocity. This occurs from the temperature dependent viscosity which varies nearly a factor of 3 over simulated film temperature range (330-370 K).

2. On the log-scale shown in **Figure 5** for the film thickness, it appears there is little difference for the three cases; however when focusing only on the cylinder, one sees about a 5% decrease in film thickness over the cylinder length. This is due to film evaporation and is reflected in an increased resistance to flow along the vertical wall. Case 3 in **Figure 4** clearly shows this effect.

We have not found any information on the PCCS pipe drainage configuration, only that cold water is introduced at the ellipsoidal apex. To understand the effect of different injection velocities, we conducted a small sensitivity analysis by assuming different pipe diameters of 0.1, 0.2, and 0.3 m with all other parameters being the same. These solutions are shown in **Figures 7-9**. The injected velocity and film thickness are related through the injected mass flow rate and pipe diameter and this dependence is clearly shown in the figures. The temperature profile along a meridian is only dependent upon the mass flow rate and mass flux as we see in equations (22) and (25), respectively, and therefore is independent of any differences in this analysis. The important observation here is that the flow adjusts within roughly 3 m from the apex to a common solution.

In the last three figures we display our baseline Case 3 and Case 6. Case 6 introduces more physical heat and mass transfer functions as used in the GASFLOW-MPI draining film model [6]. The strong effect of the evaporating film and dominate wall heat transfer is demonstrated in all three figures. Within about 7 m the film approaches its maximum value (~368 K)

resulting in the lowest kinematic viscosity value along a meridian which reduces the wall resistance. The thinning of the film due to evaporation is shown in **Figures 10-11**. These coupled effects result in increased dome velocity followed with a decreasing velocity down the cylinder. In fact, the inter-competition between heat and mass transfer along the dome results in an inflection of the velocity profile – first appears an acceleration, deceleration, a short acceleration, and then a strong deceleration all within the first 10 m.

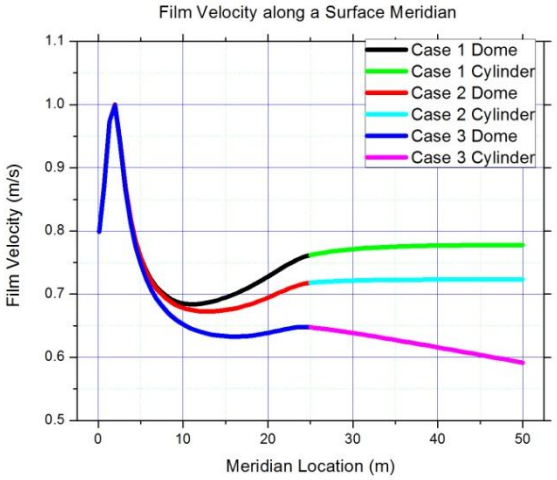

Figure 4. Film velocity from near the ellipsoidal apex along a meridian down the vertical cylinder surface for Cases 1, 2, and 3. These three cases use constant heat and mass correlations.

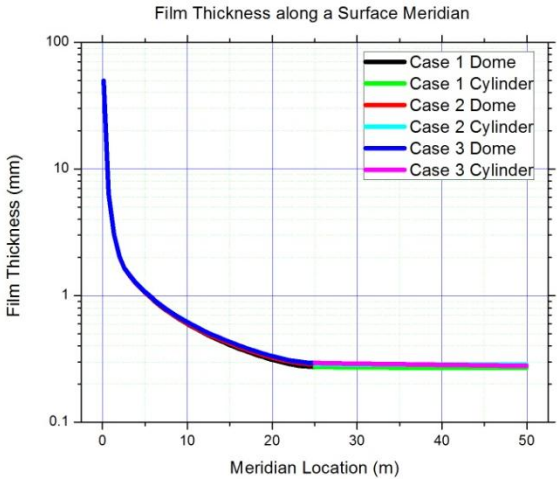

Figure 5. Film thickness from near the ellipsoidal apex along a meridian down the vertical cylinder surface for Cases 1, 2, and 3. These three cases use constant heat and mass correlations.

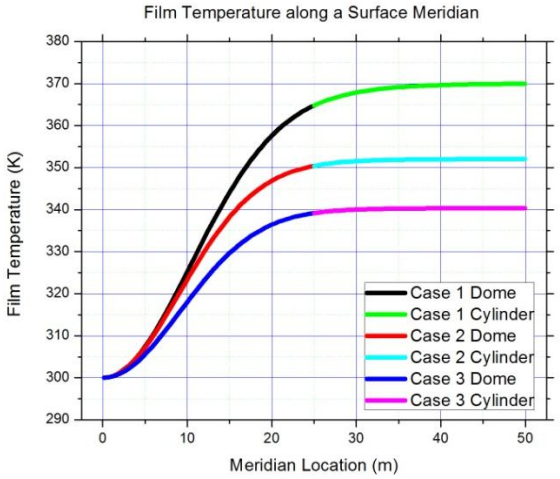

Figure 6. Film temperature from near the ellipsoidal apex along a meridian down the vertical cylinder surface for Cases 1, 2, and 3. These three cases use constant heat and mass correlations.

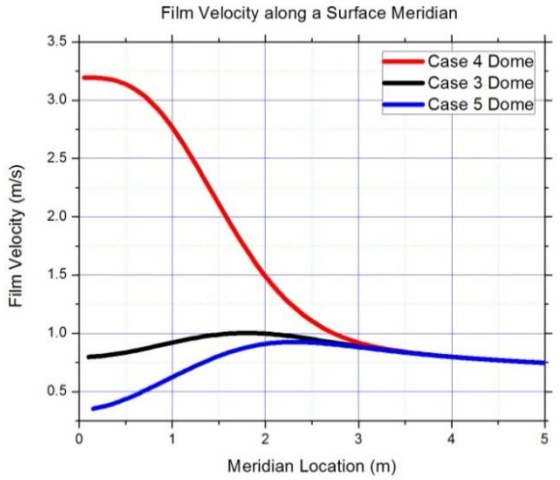

Figure 7. Film velocity from near the ellipsoidal apex along a meridian down the vertical cylinder surface for Cases 4, 3, and 5 with injection drainage pipe 0.1 m, 0.2 m, and 0.3 m.

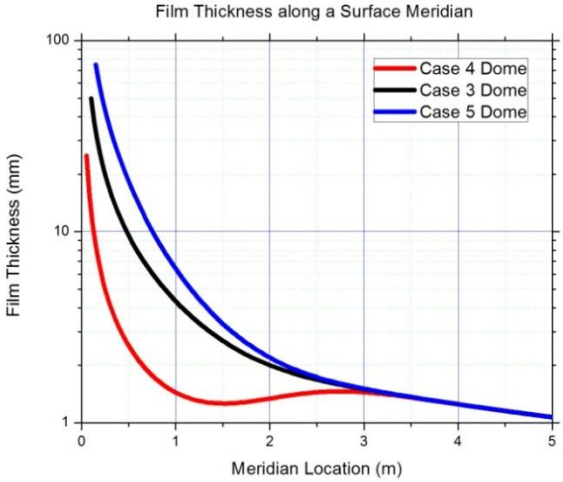

Figure 8. Film thickness from near the ellipsoidal apex along a meridian down the vertical cylinder surface for Cases 4, 3, and 5 with injection drainage pipe 0.1 m, 0.2 m, and 0.3 m.

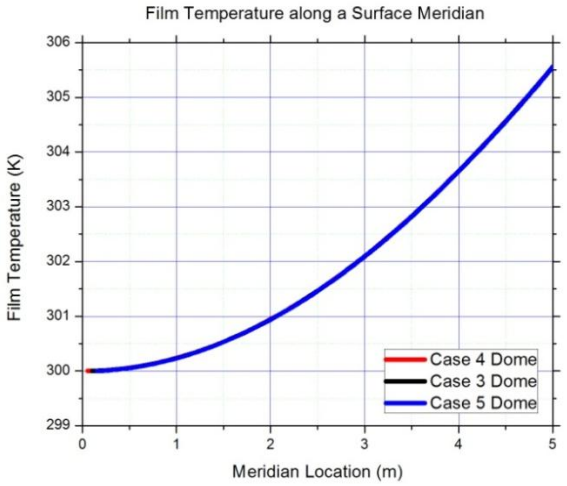

Figure 9. Film temperature from near the ellipsoidal apex along a meridian down the vertical cylinder surface for Cases 4, 3, and 5 with injection drainage pipe 0.1 m, 0.2 m, and 0.3 m.

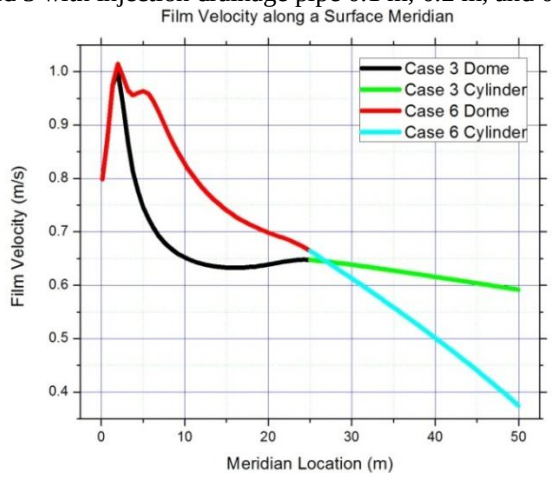

Figure 10. Film velocity from near the ellipsoidal apex along a meridian down the vertical cylinder surface for Cases 3, and 6. Case 3 uses constant heat and mass correlations while Case 6 uses functional relationships.

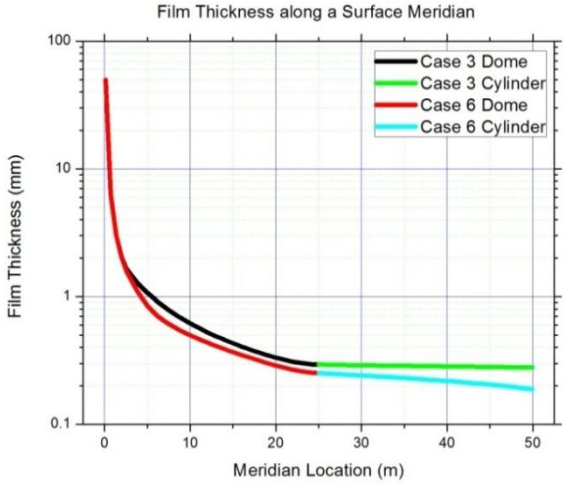

Figure 11. Film thickness from near the ellipsoidal apex along a meridian down the vertical cylinder surface for Cases 3, and 5. Case 3 uses constant heat and mass correlations while Case 6 uses functional relationships.

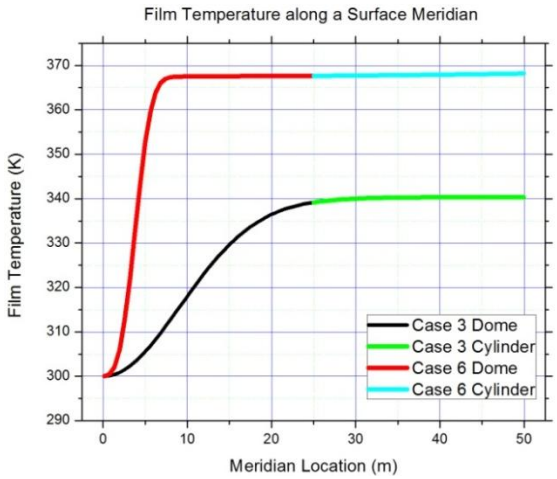

Figure 12. Film temperature from near the ellipsoidal apex along a meridian down the vertical cylinder surface for Cases 3, and 5. Case 3 uses constant heat and mass correlations while Case 6 uses functional relationships.

CONCLUSIONS

An exact numerical solution methodology, using accurate approximations to the NIST liquid water Equation of State data, has been developed, applied, and presented for the AP600 and AP1000 PCCS. The methodology can be used to validate PCCS models embedded within more complex containment codes. The procedure is developed with concern for introducing generalized physical models for the wall to film heat transfer coefficient, the film to ambient gas (air) heat transfer coefficient, and evaporating film to ambient gas relationships. There are some restrictions:

1. One-dimensional steady flow,
2. Constant wall temperature,
3. Constant ambient gas temperature, and
4. Constant ambient gas velocity.

One can easily see the coupling effects and interplay between heat and mass transfer on the draining film.

The analysis presented in this article, although referring to the geometry of the AP-1000 pressurized water reactor, is not intended to illustrate the simulation of a specific reactor design, but rather to develop a general methodology which for future code developments could become a standard validation tool.

REFERENCES

[1] Westinghouse Corporation AP1000 information document http://www.apcnean.org.ar/arch/3e139fc91ebe2e675db2194460badc7c.pdf

[2] Tills J., Notafrancesco A., and Phillips J., Application of the MELCOR Code to Design Basis PWR Large Dry Containment Analysis, Sandia National Laboratories Report, SAND2009-2858, May 2009.

[3] Huang X. and Cheng X., Modification and application of water film model in COCOSYS for PWR's passive containment cooling, , Nuclear Engineering and Design, Vol. 280, 2014, pp. 251-261.

[4] Woodcock J., Andreychek T. S., Conway L., Elicson T., Forgic A., Gresham J. A., Haessler R., O'Donnell T., Ofstun R., Spencer D. R., Sredzienski M., and Wills M., WGOTHIC Application to AP600 and AP1000, Westinghouse non-proprietary Class 3 report, WCAP-15862 Revision 1, March 2014.

[5] Sha W.T., Chien T.H., Sun J.G., and Chao B. T., Analysis of large-scale test for AP-600 passive containment cooling system, Nuclear Engineering and Design, Vol. 232, 2004, pp. 197-216.
[6] Xiao J., Travis J. and Bottoni M., Thermal-hydraulic Analysis of a Passive Containment Cooling System using Dynamic Liquid Film Model in CFD Code GASFLOW-MPI, Proceedings of the 24th International Conference on Nuclear Engineering, Charlotte, NC, 2016.
[7] Meredith K., Xin Y. and De Vries J., A Numerical Model for Simulation of Thin-Film Water Transport over Solid Fuel Surfaces, Fire Safety Science-Proceedings of the 10th International Symposium, 2011, pp. 415-428.
[8] Garcıa-Navarro P., Brufau P., Burguete J. and Murillo J., The shallow water equations: An example of hyperbolic system, Monograf´ıas de la Real Academia de Ciencias de Zaragoza, Vol 31, 2008, pp. 89–119.
[9] http://webbook.nist.gov/chemistry/fluid/
[10] Travis, J., The GASFLOW-II Saturation Curve and Suggested Alternatives, KIT Quick Look Technical Note, July 2014 (https://www.researchgate.net/profile/J_Travis)